Available online at www.sciencedirect.com

ScienceDirect

IFAC PapersOnline CONFERENCE PAPER ARCHIVE

IFAC PapersOnLine 55-1 (2022) 229–234

Application of Multi-Input Uncorrelated Periodic Signals for Identification of Active Suspension System

Ilias Kioutsoukis * **Mathias Foo** ** **Ai Hui Tan** ***

* *School of Mechanical, Aerospace and Automotive Engineering, Coventry University, CV1 5FB, Coventry, UK (e-mail: kioutsoi@outlook.com).*

** *School of Engineering, University of Warwick, CV4 7AL, Coventry, UK (e-mail: M.Foo@warwick.ac.uk)*

*** *Faculty of Engineering, Multimedia University, 63100 Cyberjaya, Malaysia (e-mail: htai@mmu.edu.my (Corresponding author))*

Abstract: Active suspension system has been widely used to improve ride comfort in passenger cars by adjusting the force between the tyre and the vehicle body such that the effect of the rough road surfaces will be minimally felt by the passengers. Control algorithms for active suspension are frequently designed using the well-known quarter-car model, which is a linear approximation of the system. In this paper, multi-input uncorrelated periodic signals are applied on a laboratory-scale active suspension system. The signals incorporate harmonic suppression allowing more accurate estimation of the frequency response functions and quantification of nonlinearities and noise. The results reveal significant amount of nonlinearities, which should be taken into account during controller design.

Keywords: active suspension systems, multi-input systems, nonlinear distortions, perturbation signals, system identification, uncorrelated signals

1. INTRODUCTION

Vehicle suspension is a vital component to lessen undesirable vibrations caused by rough road surfaces. These road surfaces induce vertical displacements to the vehicle body and a poorly designed vehicle suspension system will lead to the passenger experiencing ride discomfort, viz perceiving undesirable vehicle body movement (see e.g. Goodarzi and Khajepour (2017)).

In general, vehicle suspension systems can be classified into three categories – passive, semi-active and active (see, e.g. Huang et al. (2020)). The passive and semi-active suspension systems rely on preset dampers and springs (see, e.g. Huang et al. (2020)) and adjustable hydraulic dampers (see, e.g. Ballo (2007)), respectively, to reduce those undesirable vibrations. The tuning of these dampers and springs is often based on the traditional tuning criterion (Olley (1942); Barak (1991)). Meanwhile, the active suspension systems employ active actuators to produce relevant forces to counteract those unwanted vibrations (see, e.g. Du et al. (2020)).

Since the inception of active suspension system by the Formula One teams such as Lotus and Williams in the late 1980's and early 1990's (Howard (2001)), this technology has made its way to passenger cars due to its effectiveness in improving ride comfort. This has subsequently led to extensive research in this area to further improve the performance of the active suspension system either through key parameter optimisation approach (Lee et al. (2009); Thoresson et al. (2009a,b)) or optimal/adaptive control approach (Hrovat and Hubbard (1981); Zou et al. (2013); Deshpande et al. (2016); Mustafa et al. (2019)).

These aforementioned design methods often employ the well-known quarter-car model, which assumes negligible contribution from nonlinearities. To what extent this assumption holds depends on the physical construction of the system. It is important to verify this assumption prior to using the linear model for controller design. Hence, it is of interest to study how effective one can identify and quantify the amount of noise and nonlinearities in the active suspension system. In this paper, following the success from some previous studies (Cham et al. (2017); Tan (2018)), an identification test is performed using carefully designed perturbation signals. In particular, multi-input uncorrelated periodic signals are applied on a laboratory-scale active suspension system. The identification test serves a dual-role of frequency response function (FRF) estimation, and quantification of noise and nonlinearities. An important advantage of such an identification test is that only a single experiment is required. It also allows useful analysis to be carried out, which can provide additional guide for suspension designers.

The rest of the paper is organised as follows. The laboratory-scale active suspension system and the derivation of the quarter-car model are presented in Section 2. Section 3 discusses the design of the multi-input uncorrelated periodic signals. Results are presented in Section 4 and conclusions are given in Section 5.

10.1016/j.ifacol.2022.04.038

2. SYSTEM DESCRIPTION

The active suspension system used in this study is a laboratory-scale system developed by Quanser (Quanser (2013)) as shown in Fig. 1 (left). The dimensions of the suspension system are 30.5cm in length, 30.5cm in width and 61cm in height and its total weight is 15kg. The system comprises three masses that represent the road, tyre and body, which move along stainless steel shafts using linear bearings. These three masses are represented by silver, red and blue colour plates, respectively. The suspension system uses a brushed dc motor that is connected to a belt-drive mechanism to simulate the road surface and a brushless dc motor to implement the active suspension control.

A suspension system is usually modelled using the quarter-car model, where each of the components is represented using a classical mechanical translational component such as mass, spring or damper. The schematic of this representation is shown in Fig. 1 (right). Here, M_s and M_{us} represent the sprung mass (vehicle body) and unsprung mass (tyre), respectively. The suspension and tyre stiffnesses are denoted by K_s and K_{us}, respectively, while the suspension and tyre damping coefficients are denoted by B_s and B_{us}, respectively. The two inputs to the system are the road profile denoted by z_r and the actuating force denoted by F_c, while the two outputs are the displacements of the sprung and unsprung masses denoted by z_s and z_{us}, respectively. The values of the suspension parameters are given in Table 1 (Quanser (2013)).

Table 1. Quanser active suspension parameters (Quanser (2013))

Parameter	Value	Unit
M_s	2.45	kg
M_{us}	1.00	kg
K_s	900	N/m
K_{us}	1250	N/m
B_s	7.5	Ns/m
B_{us}	5	Ns/m

The Quanser suspension system has operating limits such that the maximum displacements of the road, body and tyre are constrained to ±22 mm, ±25.4 mm and ±19 mm, respectively, from their reference positions. The conclusions from this work are thus applicable to the case where the car is travelling at a low to moderate velocity, or to the case where the road is not too rough. This follows from the relationship between velocity, spatial frequency and cyclic frequency as explained in Tan et al. (2022).

To obtain the relationship between the input and output, often the interaction between all the variables are assumed to be linear. Using Newton's law of motion, the equations of motion of the suspension system can be derived and are given by

$$\begin{aligned} M_{us}\ddot{z}_{us} &= -B_s(\dot{z}_{us}-\dot{z}_s)+B_{us}(\dot{z}_r-\dot{z}_{us}) \\ &\quad -K_s(z_{us}-z_s)+K_{us}(z_r-z_{us})-F_c \\ M_s\ddot{z}_s &= B_s(\dot{z}_{us}-\dot{z}_s)+K_s(z_{us}-z_s)+F_c \end{aligned} \tag{1}$$

The four transfer functions $\frac{Z_{us}(s)}{Z_r(s)}$, $\frac{Z_s(s)}{Z_r(s)}$, $\frac{Z_{us}(s)}{F_c(s)}$ and $\frac{Z_s(s)}{F_c(s)}$, can be obtained by taking Laplace Transform of Eqn. (1), assuming zero initial condition. After some algebraic manipulation, these transfer functions are given by

$$\begin{aligned} \frac{Z_{us}(s)}{Z_r(s)} &= \frac{a_0s^3+a_1s^2+a_2s+a_3}{\Delta D} \\ \frac{Z_s(s)}{Z_r(s)} &= \frac{a_4s^2+a_2s+a_3}{\Delta D} \\ \frac{Z_{us}(s)}{F_c(s)} &= \frac{-M_ss^2}{\Delta D} \\ \frac{Z_s(s)}{F_c(s)} &= \frac{M_{us}s^2+B_{us}s+K_{us}}{\Delta D} \end{aligned} \tag{2}$$

where $a_0 = M_sB_{us}$ $a_1 = (B_{us}B_s+M_sK_{us})$, $a_2 = (B_{us}K_s+B_sK_{us})$, $a_3 = K_{us}K_s$, $a_4 = B_sB_{us}$ and ΔD is given by

$$\begin{aligned} \Delta D &= s^4M_{us}M_s+s^3(M_{us}B_s+M_sB_s+M_sB_{us}) \\ &\quad +s^2(M_{us}K_s+B_sB_{us}+M_sK_s+M_sK_{us}) \\ &\quad +s(B_{us}K_s+B_sK_{us})+K_{us}K_s \end{aligned}$$

By obtaining the frequency responses of Eqn. (2), one can identify the resonance of the system, which can facilitate the re-calibration of the suspension parameters or the design of relevant control strategies to reduce the effect of resonance in order to improve ride comfort.

While the above derivation with the linearity and noise-free assumption is widely used within the automotive industry, in practice it is known that suspension systems are rarely linear due to nonlinearities in the springs and dampers in particular when operating outside their *linear* regime. Moreover, the presence of noise in the sensor would often affect the overall performance of the suspension system. To our knowledge, a systematic approach in quantifying these nonlinearities and noise in suspension systems is still lacking thereby forming the motivation of this study. The effects of nonlinearities and noise can be quantified by exciting the system with perturbation signals containing certain properties. Here, the approach employed in Cham et al. (2017) is applied, where multi-input uncorrelated periodic signals are used to characterise the linear dynamics, nonlinear distortion and disturbing noise in a multi-input system, in our case the active suspension system, using simultaneous perturbation in a single experiment. A brief discussion about these signals is presented in the next section. For more details, see Cham et al. (2017).

3. MULTI-INPUT UNCORRELATED PERIODIC SIGNALS

The perturbation signals $u_1 := z_r$ and $u_2 := F_c$ are chosen as multisine signals that are uncorrelated and orthogonal with one another. Multisine signals are chosen given their flexibility in specifying their harmonics (Pintelon and Schoukens (2012)).

A multisine signal is defined by

$$u(n) = \sum_{p\in\gamma} A_p \cos\omega_p n + \phi_p \tag{3}$$

where n denotes the discrete time index, γ represents the set consisting of nonzero harmonics (excluding zero harmonics), A_p is the amplitude, $\omega_p = \frac{2\pi p}{N}$ is the normalised angular frequency with period N and ϕ_p is the phase associated with harmonic p.

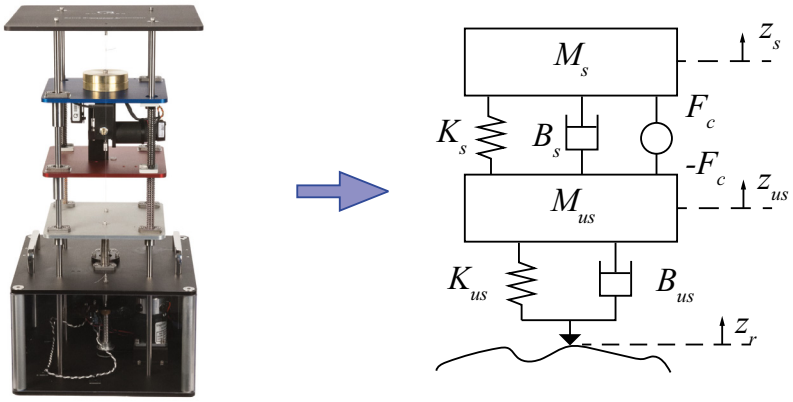

Fig. 1. Left: Laboratory-scale active suspension system. Figure is taken from Quanser (2013). Right: Schematic of the suspension system depicted using quarter-car model.

To design γ for the active suspension system, note that $N = f_s/f_{res}$, where f_s and f_{res} are the sampling frequency and frequency resolution, respectively. From Quanser (2013), $f_s = 1000$ Hz. The frequency resolution is given by $f_{res} = f_{min}/N_G$, where we set $f_{min} = 0.06$ Hz following the range suggested in Attia et al. (2017) and $N_G = 6$, which is the gap between two consecutive excited harmonics in each perturbation signal. With that $N = 1000/0.01 = 100000$.

The multisine signals have uniform Discrete Fourier Transform (DFT) magnitude at the excited harmonics as follows:

Signal A perturbing u_1: $\gamma_{SignalA} = \{1, 7, 13, ..., 39997\}$
Signal B perturbing u_2: $\gamma_{SignalB} = \{5, 11, 17, ..., 39995\}$

For practical consideration, the highest harmonics of the perturbation signals are set to $0.4N$ following the recommendation in Tan and Godfrey (2019). Signal A and Signal B are uncorrelated, as they do not have any common excited harmonics. This property allows their effects to be separated at the outputs. For example, the power at harmonic 1 can be attributed to Signal A whereas that at harmonic 5 can be attributed to Signal B. The suppression of even harmonics (i.e., the signals having no power at harmonics 2, 4, 6, ...) enables the effects of even order nonlinearities to be detected and separated. This ensures that estimates of the frequency responses will not be affected by the even order nonlinearities. Further to this, additional suppression of harmonics which are integer multiples of 3 (i.e., the signals having no power at harmonics 3, 9, 15, ...) permits the effects of odd order nonlinearities to be detected and their influence on the linear dynamic estimates to be reduced. Fig. 2 shows the two input signals that are used in this work. Note that u_1 and u_2 are scaled by factors of 0.5 and 500, respectively, to ensure that the input and output signals operate within constraints.

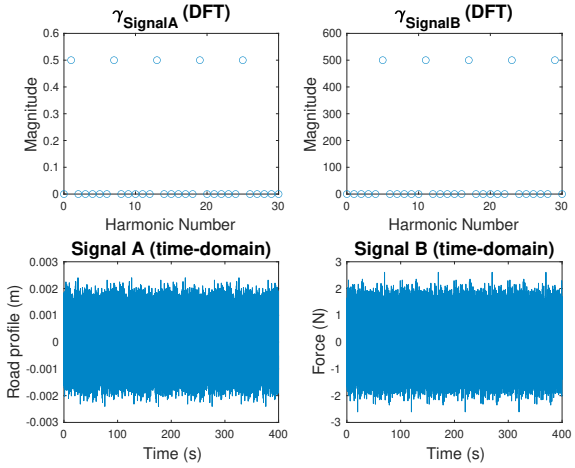

Fig. 2. DFT plots for $\gamma_{SignalA} = \{1, 7, 13, ..., 39997\}$ and $\gamma_{SignalB} = \{5, 11, 17, ..., 39995\}$ (top row) and their corresponding time-domain representations (bottom row). Left column: Road profile (Signal A). Right column: Actuating force (Signal B). For the DFT plots, only the first 30 harmonics are shown for better visualisation.

4. RESULTS

4.1 FRF of Suspension System from Transfer Functions

A typical approach in tuning the suspension system to provide the appropriate ride comfort is to identify where the resonant peaks are and then adjust the damping and/or spring coefficients to reduce those resonant peaks. To facilitate the identification of the resonant peaks, the FRF is usually used. In the case of a linear system, where the system transfer function can be derived (Eqn. (2)), the MATLAB function `bode` can be used to generate the FRF.

Substituting the relevant values of the suspension parameters given in Table 1 into Eqn. (2), the corresponding FRFs for the four transfer functions in Eqn. (2) are shown in Fig. 3. From Fig. 3, the presence of two resonant peaks at approximately between 13-15 rad/s (2.07-2.39 Hz) and 48-50 rad/s (7.64-7.96 Hz) is observed. Note that these two frequencies are close to the typical natural frequencies of the vehicle body and tyre, respectively (see e.g. Gillespie (1992); Wong (2008)).

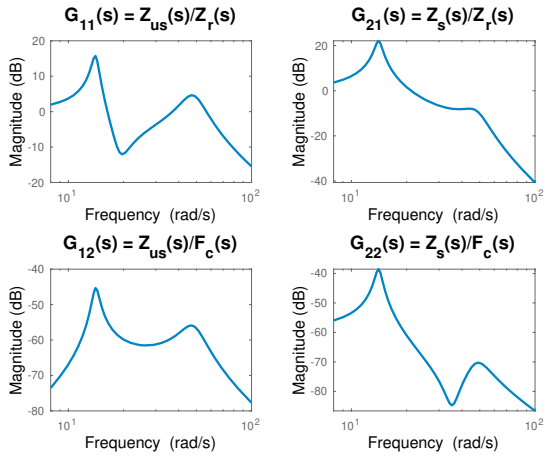

Fig. 3. FRF for the four transfer functions given in Eqn. (2) plotted using MATLAB `bode` function.

If the suspension is subject to a road surface that excites these two frequencies, the passenger will experience poor ride comfort. Thus, it is imperative that efficient suspension tuning can be developed to counter the effect of the resonant frequencies.

4.2 Estimation of FRF using Multisine Signals

The identification of the resonant frequencies to improve ride comfort is possible if the system is free from nonlinear distortion and noise. As was illustrated in the previous section, if a noise-free linear system is assumed in the derivation of the equations of motion, one can easily obtain the transfer function and compute the FRF in a straightforward manner.

The identification of the resonant frequencies can be more challenging if the contributions from nonlinearities and noise are prominent. To determine how large these contributions are, it is possible to exploit the advantage of multisine signals described by Eqn. (3). The multisine signals (i.e., Signal A and Signal B) in Section 3 can be used to estimate the FRF and quantify the contributions from nonlinearities and noise. For the latter, due to the multisine signals having certain harmonics suppressed, this special feature can be exploited to identify the contributions from nonlinearities and noise. If the system is dominantly linear and the noise contribution is negligible, the output signals when subject to the multisine inputs will only have power at the excited harmonics. The output power at the non-excited (suppressed) harmonics will provide information regarding the contributions from nonlinearities and noise. This is further discussed in Section 4.3.

In this section, the use of multisine signals to estimate the transfer function from the FRF will be explored. Following the approach in some previous studies (Cham et al. (2017); Tan (2018)), the suspension system is excited with input $z_r = u_1 =$ Signal A and $F_c = u_2 =$ Signal B as shown in Fig. 2, where they respectively represent the road profile and actuator input. The outputs $z_{us} = y_1$ and $z_s = y_2$ are measured. Four periods of the multisine signals are used, with a total measurement time of 400s. However, the initial part of the measurement is affected by transient effects in the time domain; these correspond to leakage effects in the frequency domain. It is important that these effects be removed in order for them not to distort the FRF. Thus, the measurement corresponding to the first period is discarded, leaving three steady state periods ($P = 3$) for further analysis.

The FRF is estimated by taking the DFT of both inputs and outputs and then computing $G_{ij}(z) = Y_i(z)/U_j(z)$, where $Y(z)$ and $U(z)$ represent the FRF of the output and input, respectively, while the subscripts i and j can take the values of either 1 or 2.

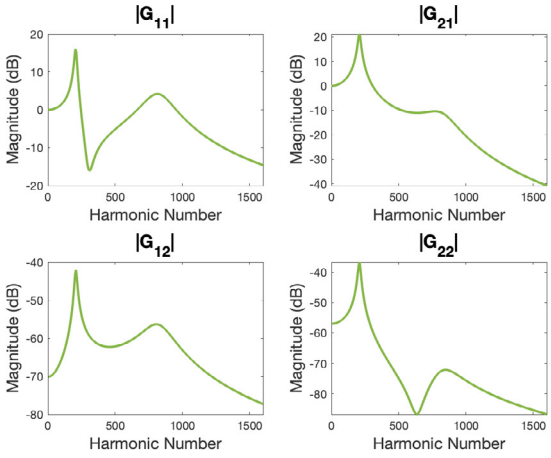

Fig. 4. FRF of the system computed using simulated output. The first 1600 harmonics are shown here for better visualisation. Black solid line: First period, Blue solid line: Second period, Red solid line: Third period, Green solid line: Average of the three individual steady state periods.

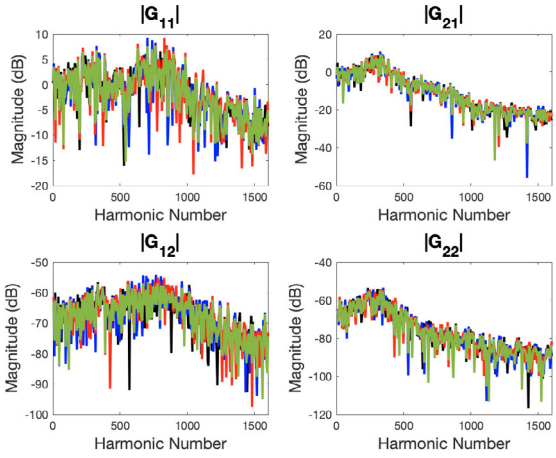

Fig. 5. FRF of the system using measured output. The first 1600 harmonics are shown here for better visualisation. Black solid line: First period, Blue solid line: Second period, Red solid line: Third period, Green solid line: Average of the three individual steady state periods.

Figs. 4 and 5 show the FRF of the four transfer functions for the simulated and measured outputs, where we consider the FRF for each period and the average of the three

periods. These respective FRFs are plotted using black, blue, red and green solid lines. For the FRFs obtained using simulated data, as expected the FRFs are smooth and have similar FRF shapes as the ones shown in Fig. 3. As there are no nonlinearities and noise considered in the simulation, the FRFs for each period and the average of the three periods are indistinguishable as they are plotted on top of each other. Notably, the two resonant frequencies are clearly observed like the ones shown in Fig. 3. With $f_{res} = 0.01$Hz, each harmonic number corresponds to $2\pi(0.01) = 0.0628$ rad/s. With that, the two resonant frequencies between 13-15 rad/s (2.07-2.39 Hz) and 48-50 rad/s (7.64-7.96 Hz) correspond to harmonic numbers 207-239 and 764-796, respectively, which is what is observed in Fig. 4. The slight difference in the FRF shapes with Fig. 3 is attributed to the conversion from continuous-time to discrete-time.

On the other hand, the four FRFs shown in Fig. 5 are significantly different from the ones obtained in Fig. 4. Each period results in different FRFs suggesting the significant contribution of noise in the system. For instance, the output 2 due to input 1 seems the noisiest with some of the FRFs from individual periods deviating the furthest from the average FRF. This could be due to the effect of the road profile being highly damped prior to being manifested as displacement of the vehicle body. In addition, the resonant frequencies are not obvious in the measured FRFs (e.g., $|G_{21}|$ and $|G_{22}|$) and this could pose challenges in suspension tuning for achieving better ride comfort.

4.3 Quantification of Nonlinearities and Noise

Here, the second role of the multisine signals, namely the quantification of the nonlinearities and noise, is discussed. The estimation of FRF in Section 4.2 reveals the 'noisy' FRFs obtained using the measured output. Whether this 'noisy' FRF is purely due to noise or results from nonlinearities will be analysed in this section.

To analyse and quantify the nonlinearities and noise present in the Quanser suspension system, we employ the output DFT computation approach used in some previous studies (Cham et al. (2017); Tan (2018)). Given that $N \times P = 100000 \times 3 = 300000$, a 300000-point DFT is computed using the 300000 time samples associated with three distinctive steady state periods. The computation of the output DFT allows the contributions from the linear, nonlinear and noise terms to be clearly separated.

With $P = 3$ and the DFT taken over three periods, the linear contributions corresponding to u_1 and u_2, respectively, appear at the following harmonics, $\{1, 7, 13, ..., 39997\} \times 3 = \{3, 21, 39, ..., 119991\}$ and $\{5, 11, 17, ..., 39995\} \times 3 = \{15, 33, 51, ..., 119985\}$.

On the other hand, the effects of even and odd nonlinear distortions appear at (non-excited harmonics $\times$ P), i.e., $\{2, 4, 6, ..., 50000\} \times 3 = \{6, 12, 18, ..., 150000\}$ and $\{3, 9, 15, ..., 49999\} \times 3 = \{9, 27, 45, ..., 149997\}$, respectively.

The harmonics at other locations, i.e. $\{1, 2, 4, ..., 149999\}$, represent the noise contribution. Like in Section 4.2, two cases are considered, where the output DFTs are computed using the simulated output from Eqn. (1) and the measured output from the Quanser suspension system. The 300000-point DFT for both simulated and measured outputs are shown in Figs. 6 and 7.

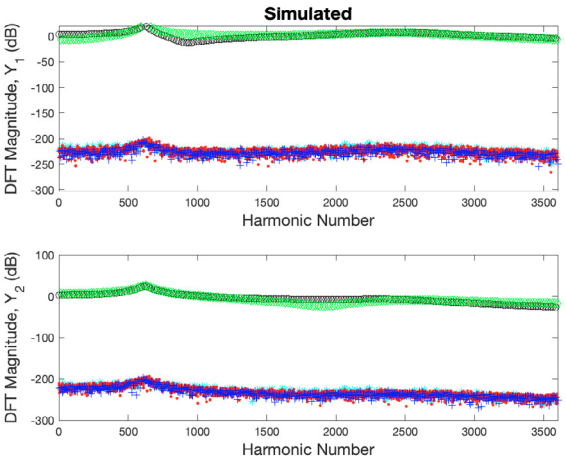

Fig. 6. DFT magnitude for simulated outputs. The first 3600 harmonics are considered for better visualisation. Black circles: Power at harmonics $\{3, 21, 39, ...119991\}$. Green diamonds: Power at harmonics $\{15, 33, 51, ...119985\}$. Blue plusses: Even order nonlinear distortion, Cyan asterisks: Odd order nonlinear distortion, Red dots: Noise.

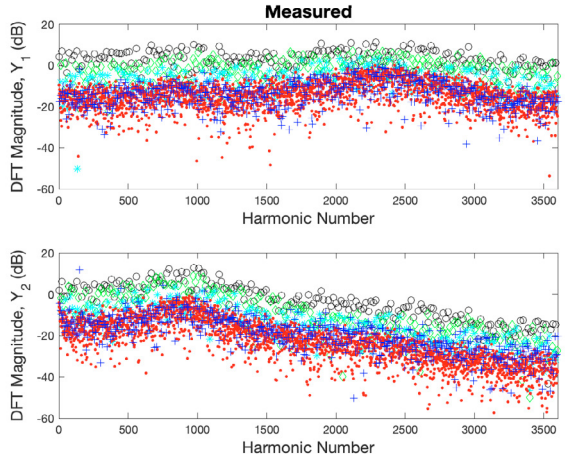

Fig. 7. DFT magnitude for measured outputs. The first 3600 harmonics are considered for better visualisation. Black circles: Power at harmonics $\{3, 21, 39, ...119991\}$. Green diamonds: Power at harmonics $\{15, 33, 51, ...119985\}$. Blue plusses: Even order nonlinear distortion, Cyan asterisks: Odd order nonlinear distortion, Red dots: Noise.

For the simulated output DFT (Fig. 6), as expected, the contributions from the nonlinear (blue plusses and cyan asterisks) and the noise (red dots) terms are negligible with their magnitudes in the range of -250 to -170 dB. Note that no noise is added to the system in obtaining the simulated output data. Thus, the presence of 'noise' (red dots) is attributed to rounding errors and not the actual noise. The contributions of the linear terms are clearly visible.

On the other hand, for the measured output DFT (Fig. 7), significant contributions from the nonlinear (blue plusses and cyan asterisks) and noise (red dots) terms are observed. For Y_1, odd order nonlinear distortion dominates over even order nonlinear distortion and noise, as the cyan asterisks are generally above the blue plusses and the red dots. The even order nonlinear distortion is roughly at the same level as the noise. In particular, the effects of odd order nonlinear distortion are about 13 dB and 8 dB below the linear effects from u_1 and u_2, respectively. The even order nonlinear distortion and noise both have a magnitude of approximately 10 dB below that of the odd order nonlinear distortion. However, for Y_2, the effects of even order nonlinear distortion are significant, especially at higher frequencies. Further investigations using different scaled inputs that operate within the constraints of the Quanser suspension system yield similar results suggesting that different input amplitudes do not significantly affect the relative contributions of noise and nonlinearities.

5. CONCLUSIONS

Traditionally, the derivation of the equations of motion for the suspension system assume that the forces acting on the mass, damper and spring are linear, and that they correspond to the acceleration, velocity and displacement, respectively. This enables the derivation of the transfer functions allowing the computation of FRF to identify the resonant frequencies such that an appropriate tuning approach can be undertaken to improve ride comfort. In this study, using multisine input signals, the effects of nonlinearities and noise in a suspension system were analysed and quantified using measured outputs from a laboratory-scale suspension system. The results show that the effects of nonlinearities and noise are significant to the extent of eluding the resonant frequencies that were previously identified using the linear model. These findings also suggest that some additional measures need to be taken when developing tuning approaches. These measures include, but are not limited to, nonlinearities and noise compensation techniques and the use of nonlinear models.

ACKNOWLEDGEMENTS

Financial support from the Ministry of Higher Education, Malaysia, under the Fundamental Research Grant Scheme FRGS/1/2021/TK0/MMU/02/5 “Real-Time Input Design Method with Machine Learning for Cyber-Physical System Identification” is gratefully acknowledged. IK and MF would like to acknowledge Ian Bates from Coventry University for the assistance provided related to the use of the Quanser active suspension system.

REFERENCES

Attia T., Kochersberg K., Bird J., and Southward S.C., System identification and optimal control of half-car active suspension system using a single noisy IMU with position uncertainty. *Proc. ASME, Dyn. Sys. Contr. Conf.*, 58288, 2017.

Ballo I., Comparison of the properties of active and semiactive suspension. *Veh. Syst. Dyn.*, 45:1065–1073, 2007.

Barak P., Magic numbers in design of suspensions for passenger cars. *SAE Paper*, 911921, 1991.

Cham C.L., Tan A.H. and Tan W.H., Identification of a multivariable nonlinear and time-varying mist reactor system. *Control Eng. Pract.*, 63:13–23, 2017.

Deshpande V.S., Shendge O. and Phadke S., Nonlinear control for dual objective active suspension systems. *IEEE Trans. Intell. Transp. Syst.*, 18:1–10, 2016.

Du H., Li W., Ning D., Sun S. and Zhu Q.M., *Advanced Seat Suspension Control System Design for Heavy Duty Vehicles.* Academic Press, 2020.

Gillespie T.D., *Fundamentals of vehicle dynamics.* SAE Technical Paper, 1992.

Goodarzi R., and Khajepour A., *Vehicle Suspension System Technology and Design.* Morgan & Claypool Publishers, 2017.

Howard K., Active suspension. Available: https://www.motorsportmagazine.com/archive/article/december-2001/69/active-suspension, 2001.

Hrovat D. and Hubbard M., Optimal vehicle suspensions minimizing RMS rattle space, sprung mass acceleration and jerk. *Trans. of the ASME*, 103:228–236, 1981.

Huang Y., Na J., Wu X. and Gao G., Robust adaptive parameter estimation and control for vehicle active suspension systems. In *Vibration Control and Actuation in Large-Scale Systems.* Academic Press, 225–252, 2020.

Lee H.G., Won C.J. and Kim J.W., Design sensitivity analysis and optimization of McPherson suspension systems. *World Congress on Engineering, London, UK, 1-3 July*, 1532–1537, 2009.

Mustafa G.I.Y, Wang H. and Tian Y., Model free adaptive fuzzy logic control for a half car active suspension system. *Stud. Inform. Control.*, 28:13–24, 2019.

Olley M., *Spring suspension.* US Patent, 1942.

Pintelon R., and Schoukens J., *System Identification: A Frequency Domain Approach.* John Wiley & Sons Inc., 2012.

Quanser, *Active Suspension System: User Manual.* Quanser Corporation, 2013.

Tan A.H., Multi-input identification using uncorrelated signals and its application to dual-stage hard disk drives. *IEEE Trans. Magn.*, 54: Article No. 9300604, 2018.

Tan A.H., and Godfrey K.R., *Industrial Process Identification: Perturbation Signal Design and Applications.* Springer, 2019.

Tan A.H., Foo M. and Ong D.S., Road classification using built-in self-scaling method of Bayesian regression. *J. Sound Vibr.*, 516: Article No. 116523, 2022.

Thoresson M.J., Uys P.E., Els P.S. and Snyman J.A., Efficient optimisation of a vehicle suspension system, using a gradient-based approximation method, Part 1: mathematical modelling. *Mathl. Comput. Modelling*, 50:1421–1436, 2009a.

Thoresson M.J., Uys P.E., Els P.S. and Snyman J.A., Efficient optimisation of a vehicle suspension system, using a gradient-based approximation method, Part 2: optimisation results. *Mathl. Comput. Modelling*, 50:1437–1447, 2009b.

Wong J.Y., *Theory of Ground Vehicles.* John Wiley & Sons Inc., 2008.

Zou Y., Shi J.H., Dong G.L., Wei G. and Hu X.S., Optimal energy control strategy design for a hybrid electric vehicle. *Disc. Dyn. Nat. Soc.*, 292–297, 2013.